



## ORIGINAL RESEARCH

# Global Landscape of Native Protein Complexes in *Synechocystis* sp. PCC 6803



Chen Xu<sup>1</sup>, Bing Wang<sup>1</sup>, Lin Yang<sup>1</sup>, Lucas Zhongming Hu<sup>2</sup>, Lanxing Yi<sup>1</sup>,  
 Yaxuan Wang<sup>1</sup>, Shenglan Chen<sup>1</sup>, Andrew Emili<sup>2,3</sup>, Cuihong Wan<sup>1,\*</sup>

<sup>1</sup> School of Life Sciences and Hubei Key Laboratory of Genetic Regulation and Integrative Biology, Central China Normal University, Wuhan 430079, China

<sup>2</sup> Donnelly Centre for Cellular and Biomolecular Research, University of Toronto, Toronto, ON M5S 2E8, Canada

<sup>3</sup> Departments of Biochemistry and Biology, Boston University, Boston, MA 02215, USA

Received 8 June 2019; revised 4 April 2020; accepted 12 June 2020

Available online 24 February 2021

Handled by Yu Xue

## KEYWORDS

Protein–protein interaction;  
 Cyanobacterium;  
 Co-fractionation;  
 Photosynthesis;  
 Function prediction

**Abstract** *Synechocystis* sp. PCC 6803 (hereafter: *Synechocystis*) is a model organism for studying **photosynthesis**, energy metabolism, and environmental stress. Although known as the first fully sequenced phototrophic organism, *Synechocystis* still has almost half of its proteome without functional annotations. In this study, by using **co-fractionation** coupled with liquid chromatography–tandem mass spectrometry (LC-MS/MS), we define 291 multi-protein complexes, encompassing 24,092 **protein–protein interactions** (PPIs) among 2062 distinct gene products. This information not only reveals the roles of photosynthesis in metabolism, cell motility, DNA repair, cell division, and other physiological processes, but also shows how protein functions vary from bacteria to higher plants due to changes in interaction partners. It also allows us to uncover the functions of hypothetical proteins, such as SII0445, SII0446, and SII0447 involved in photosynthesis and cell motility, and SII1334 involved in regulation of fatty acid biogenesis. Here we present the most extensive PPI data for *Synechocystis* so far, which provide critical insights into fundamental molecular mechanisms in cyanobacteria.

## Introduction

Cyanobacteria represent the phylogenetic ancestors of chloroplasts from present-day plants [1,2]. The oxygen generated by

oxygenic photosynthesis is believed to change the atmospheric composition and promote biodiversity on earth [3]. *Synechocystis* is a unicellular photoautotrophic cyanobacterium, which is an ideal model organism for studying photosynthesis, energy metabolism, and environmental stress [4,5]. The genome of *Synechocystis* was sequenced in 1996 [6], and its proteome has also been well analyzed in the last two decades [7,8]. However, about two-thirds of its proteins in the UniProt database are listed as “hypothetical”, and most of them lack functional annotation.

\* Corresponding author.

E-mail: [ch\\_wan@mail.ccnu.edu.cn](mailto:ch_wan@mail.ccnu.edu.cn) (Wan C).

Peer review under responsibility of Beijing Institute of Genomics, Chinese Academy of Sciences / China National Center for Bioinformatics and Genetics Society of China.

<https://doi.org/10.1016/j.gpb.2020.06.020>

1672-0229 © 2022 The Authors. Published by Elsevier B.V. and Science Press on behalf of Beijing Institute of Genomics, Chinese Academy of Sciences / China National Center for Bioinformatics and Genetics Society of China. This is an open access article under the CC BY license (<http://creativecommons.org/licenses/by/4.0/>).

Completion of many important biological functions relies on stable physical interactions between two or more proteins. Protein–protein interactions (PPIs) are critical to understand the fundamental molecular biology of organisms, which can be used for predicting annotation, finding new drug targets, and so on [9]. However, information on *Synechocystis*'s PPIs is quite a deficiency. Researchers have tried to analyze PPIs by using yeast two-hybrid (Y2H) assays and several kinds of prediction algorithms [10–13]. However, in the STRING database, only 6510 PPIs involving 1876 proteins in *Synechocystis* were annotated with “experiments” until January 2019, which contained PPIs with relevant information transferred from other organisms. Even for those well-known *Synechocystis* protein complexes, for example, the photosystem II (PSII) assembly, putative assembly factors remain to be identified to fully understand the biogenesis process [14,15]. The phototactic movement of cells is influenced by the motility apparatus and light, but the link between photoreceptors and the motility apparatus remains uncertain [16,17]. Thus, globally mapping the PPI connectivity network of *Synechocystis* can provide a useful resource for functional inference.

High-throughput methods have been applied to systematically determine global protein interaction maps in many organisms, such as *Escherichia coli*, fly, worm, yeast, and human [18–21]. Several techniques have been developed to identify protein complexes at the proteome scale, e.g., Y2H, affinity purification mass spectrometry (APMS), and co-fractionation coupled with mass spectrometry (CoFrac-MS). Among these methods, CoFrac-MS can rapidly detect hundreds of endogenous macromolecular complexes composed of multiple stably-associated proteins under near native physiological conditions [22]. CoFrac-MS has been broadly used to identify PPIs at the proteome scale [23–25].

To reveal PPIs and uncover novel biological functions, we applied CoFrac-MS to analyze the protein complexes of *Synechocystis*. In this work, we predict the membership of 291 protein complexes containing 24,092 highly confident PPIs among 2062 proteins. This network facilitates our comprehensive understanding of the relationship between photosynthesis and other functions, such as carbohydrate metabolic process, signal transduction, ion transport, cell division, and transcription. In addition, we applied the PPI information to predict and confirm the new functions of proteins, such as SII0445, SII0446, SII0447, and SIII334. This work allows us to comprehensively understand the fundamental molecular organizations and mechanisms of *Synechocystis* and other cyanobacterial species.

## Results and discussion

### Workflow for protein complex identification in *Synechocystis*

The experimental workflow is similar to previous work (Figure 1A) [20]. Total protein mixtures were extracted from *Synechocystis*, separated by ion-exchange chromatography (IEX), size-exclusion chromatography (SEC), or sucrose density gradient centrifugation (SDGC), and analyzed by LC-MS/MS. SEC is advantageous for distribution of protein according to different molecular weight (MW) [24]. However, SEC is not sufficient to resolve protein complexes with MW beyond its valid separation range. To improve separation efficiency, we applied IEX as an additional separation technique. These two techniques are

complementary in which IEX can resolve protein complexes that are not distinguishable during SEC (Figure S1).

In total, 181 fractions were collected, and 2906 proteins were confidently identified (Table S1). Proteins were separated effectively according to their MW and isoelectric point (pI) (Figure S2). The value of Rapp, the ratio of Mapp (apparent molecular mass, Figure S3) to Mmono (predicted molecular mass of the monomer), was evaluated to estimate whether a protein was involved in a stable heteromeric complexes on the SEC column [26,27].  $Rapp \geq 2$  was used to classify proteins predicted to be within a complex, while  $Rapp \leq 0.5$  suggested that protein degradation occurred during the protein extraction process (Figure 1B). The reproducibility between biological replicates was confirmed by Pearson correlation coefficient analysis of the profiles of spectral counts recorded for each identified protein (Figure 1C).

The components of stable protein assemblies co-elute together and can be detected by CoFrac-MS, while unstable assemblies become dispersed and so present unsatisfactory correlation profiling [19]. For example, photosystem components, NAD(P)H-quinone oxidoreductase, RubisCO complexes, and C-phycoyanin, tend to have a consistent correlation profiling (Figure S4). These protein elution profiles in turn confirm that CoFrac-MS is a powerful tool to explore global protein interactions in organisms. We confirm the final set of PPIs by machine learning using Elution Profile-based Inference of Complexes (EPIC) [28], with the classifier trained based on 47 reference ‘gold standard’ macromolecules annotated in the UniProt and IntAct databases (Table S2). The output of the prediction procedure was used to predict the components of multi-protein complexes (Figure 1D, Figure S5).

From this analysis, 2214 proteins were predicted to participate in 35,028 highly confident pairwise associations (Table S3). Our study provides the most extensive physical interaction network for *Synechocystis* to date, with ~ 10% of the putative PPIs overlapping with previously reported pairs in a curation database, such as STRING and IntAct (Figure 2A). We compared the distribution of interactions/degrees, which reflects the critical connectivity of each protein in the network [29] we found with that reported for several different model organisms, such as *E. coli*, *Saccharomyces cerevisiae*, *Arabidopsis thaliana*, and *Homo sapiens*, according to the mentha database [30]. We observed that most of the proteins in *Synechocystis* tend to have low degrees, and that interacting proteins tend to be annotated to different metabolism pathways in *Synechocystis*, such as organonitrogen, aromatic, and cellular nitrogen compound biosynthetic process (Figure 2B, Figure S6). In contrast, ribosomes and heat shock proteins present high degrees in our dataset and are conserved across different species (Figure 2B); for example, DnaK1 and DnaJ occupy important positions in metabolism [31]. Other conserved proteins tend to have high degrees [32]. Additionally, proteins that have homologs in *E. coli*, *A. thaliana*, *H. sapiens*, or *S. cerevisiae* were found to have higher degrees than proteins unique to *Synechocystis* (Figure 2C).

### Photosynthetic apparatus involved in multiple metabolic pathways

As a model organism to study photosynthesis, *Synechocystis* has a classical photosystem structure containing photosystem I

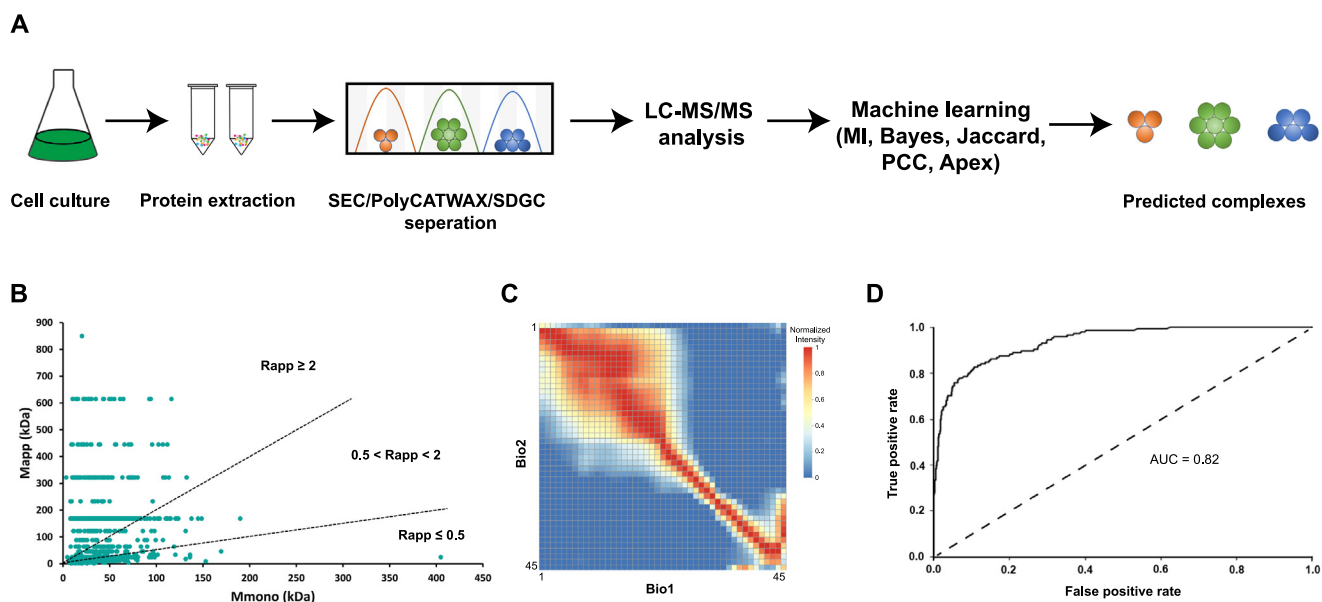


**Figure 1** Workflow for the identification of native protein complexes

**A.** Schematic diagram of co-fractionation, LC-MS/MS, and machine learning. Lysates containing a mixture of protein complexes were produced, and then separated by SEC, IEX, or SDGC. Proteins in each fraction were digested with trypsin and analyzed using nano-LC-MS/MS. Putative PPIs were predicted by machine learning using EPIC toolkits. **B.** The calculation of Rapp, which can accurately reflect the oligomerization state of proteins. A protein with  $Rapp \geq 2$  means that it has interactions with other proteins. **C.** Heatmap of the Pearson correlation coefficients of the protein quantification signals in two SEC biological replicates. **D.** Receiver operating characteristic curve of machine learning. SEC, size-exclusion chromatography; IEX, ion-exchange chromatography; SDGC, sucrose density gradient centrifugation; LC-MS/MS, liquid chromatography-tandem mass spectrometry; PPI, protein-protein interaction; EPIC, Elution Profile-based Inference of Complexes; Rapp, the ratio of Mapp to Mmono; Mapp, apparent molecular mass; Mmono, predicted molecular mass of the monomer; AUC, area under the curve.

(PSI), PSII, cytochrome  $b_6f$  complexes, and ATP synthase complexes [5]. There are 70 proteins annotated with photosynthesis, and 760 proteins were found to have direct interactions with these proteins in our dataset (Table S4). Photosynthesis-associated proteins were clustered into 26 different groups based on their functions, including phosphorelay signal transduction system, potassium ion transport, DNA repair, cell division, carbohydrate metabolic process, transcription, DNA-templated, translation, chemotaxis, and cell redox homeostasis (Figure 2D). The results indicate how photosynthesis influences many critical biological processes other than photosynthetic carbon fixation. For example, we observed that several CheA-like proteins interact with photosynthetic core proteins in our database. These CheA-like proteins have phosphorelay sensor kinase activities and participate in cellular chemotaxis [16]. These observations suggest that cells might control motility direction by regulating the state of CheA-like proteins through phosphorelay in photosynthesis.

Protein transport Sec complexes also had an association with photosynthetic proteins [14]. The subunits SecD and SecF might participate in the PSII assembly process by interacting with different PSII core proteins with a similar function as SecY (Figure 2D). SecY is the main transmembrane subunit of preprotein translocase that is essential for PSII assembly by interacting with YidC insertase to facilitate co-translational pD1 insertion [33,34]. In our dataset, ChlD, a chlorophyll biosynthesis protein, was also observed to interact with SecD, indicating that it might be functional to deliver chlorophyll to the newly synthesized pD1, playing a similar

role as ChlG (Figure 2D) [34]. Besides, although we observed that most proteins interacting with photosynthetic proteins are mainly localized in the cytoplasm, these proteins have possible roles in mobility or secretion according to localization identification results [35]. These results provide a clue for understanding how photosynthetic proteins may transmit signals and influence the physiological metabolism of cells.

### The landscape of native protein complexes in *Synechocystis*

From the highly confident protein pair assignments from machine learning, we predicted 291 protein complexes with 24,092 PPIs using the ClusterONE clustering algorithm [36], which is implemented in the EPIC software. The set of predicted putative complexes contains well-known and highly-conserved complexes, such as PSI, RubisCO, and NADH dehydrogenase (Figure 3; Table S5). The functions of predicted complexes involved in photosynthesis, carbon absorption, nitrogen fixing, and electron transfer were also deduced. Besides, we also observed protein assemblies with unclear molecular function annotations, such as clustered regularly interspaced short palindromic repeats (CRISPR) system proteins SII7085–SII7090, photosystem proteins SII0144–SII0149, and ATP-dependent zinc metalloprotease FtsH complexes (Figure 3).

According to the computational analysis, *Synechocystis* has three types of CRISPR/CRISPR-associated (Cas) systems, but their exact functions remain unclear [37–39]. In our dataset, we found that some CRISPR3 proteins can form stable com-

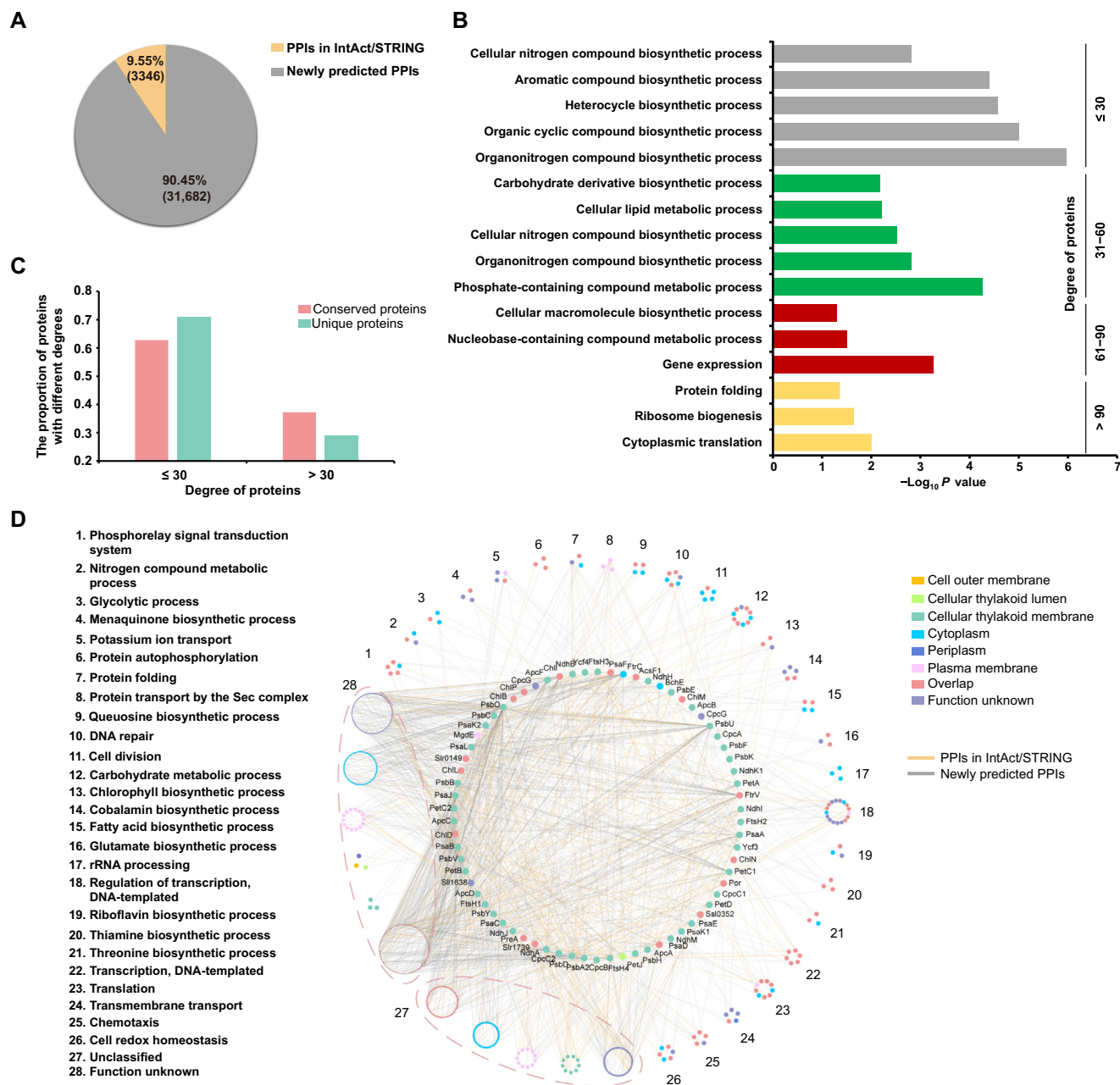


**Figure 2** The characteristics of predicted PPIs

**A.** Pie chart showing the overlap of predicted co-complexed PPIs with PPIs from IntAct and STRING databases. **B.** GO analysis of proteins with different degrees. Degree means the number of edges that one protein links to other proteins in the network ( $P < 0.05$ ). **C.** The degree distributions of conserved proteins and unique proteins in *Synechocystis*. The conserved protein refers to the protein showing homology with proteins in *E. coli*, *A. thaliana*, *H. sapiens*, and *S. cerevisiae*. **D.** The photosynthesis-associated proteins classified based on their functions. Each cluster has three or more proteins aggregated with the same GO term. Node colors represent the subcellular localizations of proteins. “Overlap” means that the proteins have multiple subcellular localization annotations. GO, Gene Ontology.

plexes, while protein interactions between different CRISPR systems were also observed (Figure S7). These results suggest that different types of CRISPR scanning systems coordinate with each other to defend cells from virus and plasmid invaders rather than functioning independently.

The hypothetical proteins Slr0144–Slr0149 are located on the thylakoid membrane and contain putative bilin binding domains, 4-vinyl reductase (V4R) domains, and 2Fe-2S cluster binding domains. They are mainly involved in photosynthetic

repair [40]. The interactions of Slr0144–Slr0149 were independently validated by APMS (Figure S8).

Among the novel predicted complexes, we found that hypothetical proteins, SlI0445, SlI0446, and SlI0447 formed a stable association with pilus assembly proteins, Slr2015 and Slr2018, as well as with photosystem complexes. The physical interactions between SlI0445 and photosynthetic proteins were verified by APMS experiments (Table S6); APMS revealed additional candidate partners, presumably because different



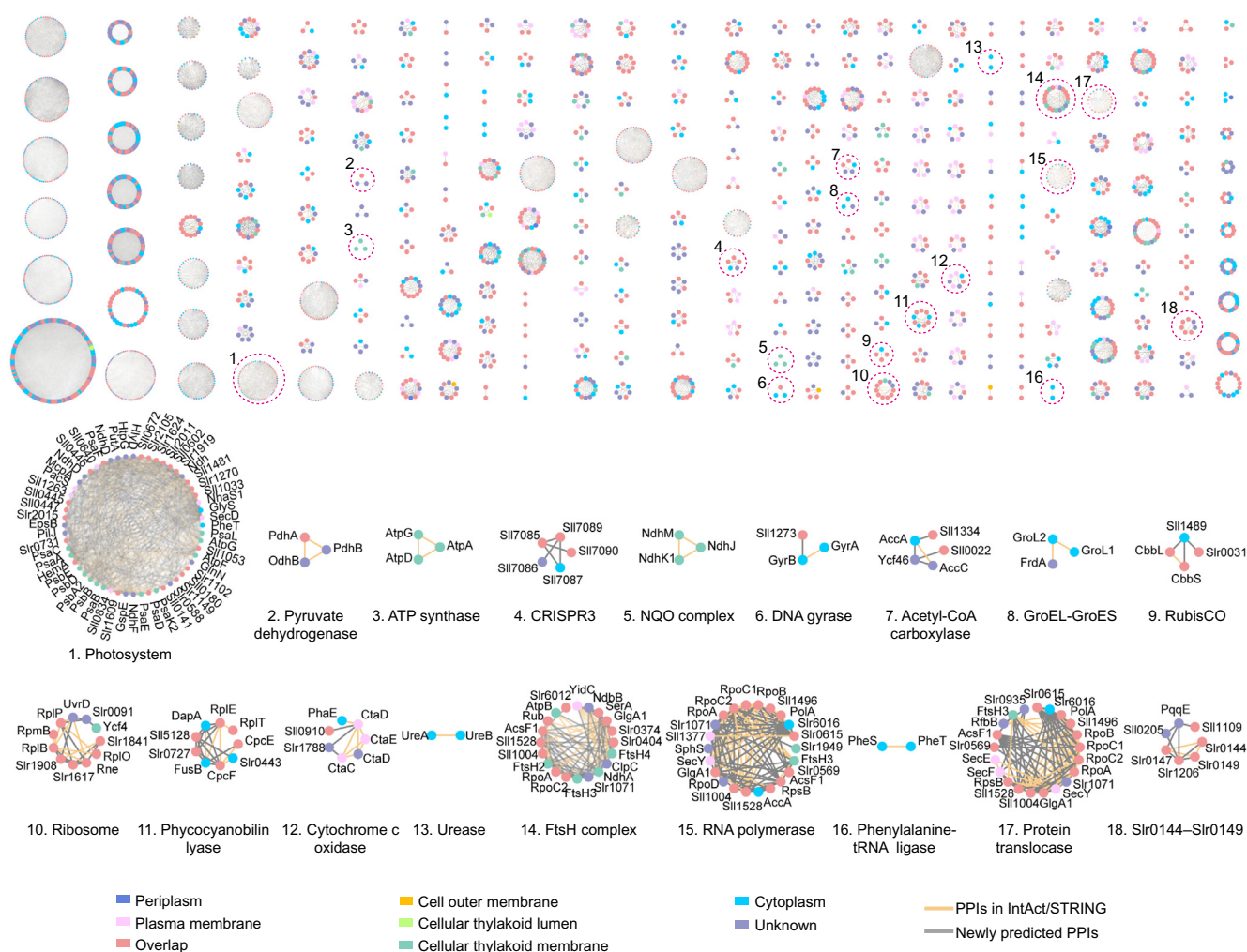


**Figure 3 Protein complex map of *Synechocystis***

The top part shows the global landscape of 291 *Synechocystis* protein complexes. The protein nodes are colored according to their subcellular localizations. “Overlap” indicates that the complex components have multiple subcellular localization annotations. The bottom part presents some of the known protein complex clusters, such as photosystem, ATP synthase, and ribosome, which are annotated with their name or abbreviation. Yellow lines between proteins indicate the interactions found in public databases, while gray lines indicate the interactions only reported in this study.

methods tend to catch different physical interactions [41]. It is worth mentioning that Slr2015 and Slr2018 interacted with Sll0445 by combining the results from co-fractionation and APMS (Figure S8). Slr2018 is located at the plasma membrane and is known to be regulated by SYCRP1, which is a cAMP receptor that influences cell motility in *Synechocystis* [42]. While Slr2018 shows no homology with other proteins, its cognate gene is adjacent to genes encoding Slr2015, Slr2016, and Slr2017, which have roles in pilus morphology and motility. These proteins were predicted to form protein complexes with photosynthetic proteins (Figure 3) [43], our results reveal a close connection presents between photosynthesis and cell motility in *Synechocystis*.

### Conserved complexes recruit different protein members across species

Half of our predicted protein complexes have conserved homologs in other species, like *A. thaliana* or *E. coli*, while the rest

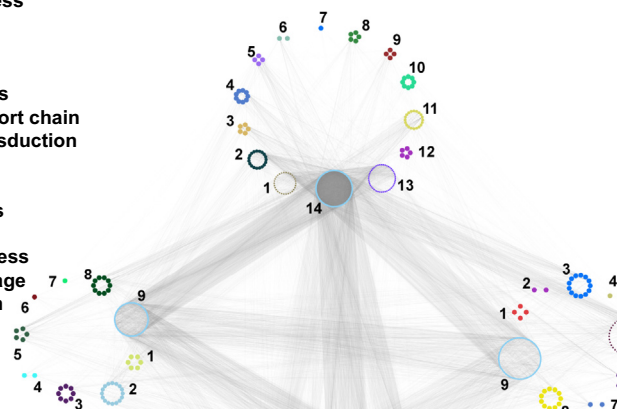
are unique to *Synechocystis* (Figure S9). The conservation of protein complexes was evaluated based on the number of proteins with known homologs in each complex. On average, the predicted protein complexes in *Synechocystis* have a higher similarity with plants (e.g., *A. thaliana*) and bacteria (e.g., *E. coli*) as compared to eukaryotes (e.g., *H. sapiens* and *S. cerevisiae*), presumably reflecting overlap with the metabolic feature of Gram-negative bacteria and the photosynthetic apparatus of green plants. There are 920 proteins and 813 proteins with homologs in *E. coli* and *A. thaliana*, respectively (Table S7).

To examine the evolutionary relationship of *Synechocystis* assemblies with those of *A. thaliana* and *E. coli*, we separated our predicted complexes according to homology. The components of the predicted complexes were divided into four parts: unique in *Synechocystis*, homologous to *E. coli*, homologous to *A. thaliana*, and homologous to both *E. coli* and *A. thaliana* (Figure 4A). Proteins having homologs in both *E. coli* and *A. thaliana* retained functions in energy metabolism, organic syn-

## A

Unique in *Synechocystis*

1. Cofactor biosynthetic process
2. Proteolysis
3. RNA biosynthetic process
4. Homeostatic process
5. Antibiotic metabolic process
6. Respiratory electron transport chain
7. Two-component signal transduction system (phosphorelay)
8. Chemotaxis
9. Mannose metabolic process
10. Secretion by cell
11. Phosphate metabolic process
12. Protein-chromophore linkage
13. Regulation of transcription
14. Function unknown

Homologous to *A. thaliana*

1. Pigment biosynthetic process
2. Protein-chromophore linkage
3. Two-component signal transduction system (phosphorelay)
4. Proton transport
5. Oxidation-reduction
6. Generation of precursor metabolites and energy
7. Homeostatic process
8. Photosynthesis
9. Function unknown

Homologous to *E. coli*

1. Di-, tri-valent inorganic cation transport
2. Polysaccharide metabolic process
3. Protein transport
4. Pyridoxine biosynthetic process
5. tRNA modification
6. Carbohydrate biosynthetic process
7. Cell wall macromolecule metabolic process
8. Coenzyme biosynthetic process
9. Function unknown

Homologous to both *E. coli* and *A. thaliana*

1. Nitrogen compound biosynthetic process
2. Generation of precursor metabolites and energy
3. Organic acid biosynthetic process
4. ncRNA metabolic process
5. Serine family amino acid metabolic process
6. Monosaccharide metabolic process
7. Secondary metabolic process
8. Purine nucleotide metabolic process
9. Cellular carbohydrate biosynthetic process
10. RNA processing
11. Coenzyme metabolic process
12. Oxidation-reduction
13. Translation
14. Function unknown

## B

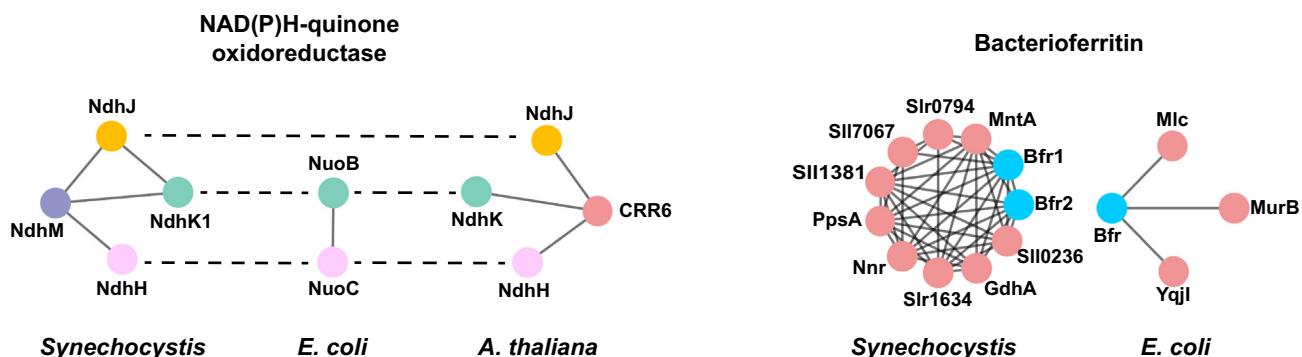


**Figure 4** Properties of evolutionarily conserved protein complexes

A. Proteins with homologs in either *E. coli* or *A. thaliana*, in both *E. coli* and *A. thaliana*, or unique in *Synechocystis* were grouped according to their representative biological processes. B. Examples of PPI variations of NAD(P)H-quinone oxidoreductase (left) and bacterioferritin (right) across species. Physical interactions in *E. coli* and *A. thaliana* were collected from the mentha database. InParanoid orthologs of two or three species are depicted with the same colors. Proteins without homologs in other species are shown in red.

thesis, protein expression, and cellular regulation, which are considered as basic activities conserved across most species. Proteins with homologs in *A. thaliana* were mainly related to photosynthesis and pigment biosynthesis, which is consistent

with the fact that one of the most remarkable features shared between *Synechocystis* and *A. thaliana* is photosynthetic capacity. Proteins with homologs in *E. coli* were primarily associated with the polysaccharide production, protein transport, and

coenzyme biosynthesis, reflecting the similarities of *Synechocystis* and *E. coli* in terms of cellular structure and physiological properties [44,45].

Notably, the terms of oxidation–reduction, homeostatic process, and two-component signal transduction system (phosphorelay) were assigned to more than one of these four groups. However, proteins that performed these functions and their interaction partners were different (Figure 4A). For example, proteins annotated as “oxidation–reduction” that have homologs in both *A. thaliana* and *E. coli* mainly participate in the “generation of precursor metabolites and energy” and “cellular respiration” processes, while proteins annotated as “oxidation–reduction” that have homologs only in *A. thaliana* are mainly associated with photosynthesis (Figure S10).

Here, we identified 14 NAD(P)H:quinone oxidoreductases (NQOs) (Table S1), of which 11 form complexes in our final network (Table S5). The components and functions of NQOs are not entirely consistent in different species [51]. The subcellular localizations of NQOs, which mediate electron transfer and shuttling of electrons from donors to quinones, are different in *E. coli*, *A. thaliana*, and *Synechocystis* [46–48]. NQOs are on the plasma membrane and participate in the respiratory process in *E. coli*, whereas the same complexes are found primarily on the thylakoid membrane in *A. thaliana* and *Synechocystis*, where they engage in the process of photosynthetic electron transport [49,50]. We compared the PPIs of partial NQOs in *E. coli*, *A. thaliana*, and *Synechocystis*. We found that NdhM is only found in *Synechocystis*, while NdhJ is present in both *A. thaliana* and *Synechocystis*. In contrast, NdhK and NdhH are conserved in all three species (Figure 4B, left).

These results indicate that some components of the NQOs participate in the respiratory electron transport while others may have evolved new functions. For example, NdhJ and NdhM might be involved in photosynthesis in *A. thaliana* and *Synechocystis*. The appearance of homologs with roles in oxidation–reduction in *A. thaliana* can be a result of adapting to photosynthetic damage or participation in electron transport in *Synechocystis*. Reactive oxygen species (ROS) produced by aerobic metabolism in photoautotroph are disposed of by antioxidants [52,53]. The presence of new enzymes with roles in oxidation–reduction can potentially reduce the influence of oxidative stress.

Bacterioferritin (Bfr) is an iron-storage protein, whose ferroxidase center binds to and oxidizes  $\text{Fe}^{2+}$  to  $\text{Fe}^{3+}$  by oxygen. The PPIs of Bfr proteins were studied and compared across three species. Intriguingly, no ortholog was found in *A. thaliana*, and only one ortholog (*i.e.*, Bfr) was found in *E. coli* (Figure 4B, right), suggesting that other proteins might perform this function in *A. thaliana*. Photoautotrophic microorganisms tend to have a massive demand for inorganic ions, such as Fe and Mn. Because inorganic ions are usually deficient in the open ocean, a unique mechanism for microbes to transport and store ions is required [54,55]. The presence of two Bfr orthologs in *Synechocystis* indicates that it may have an additional requirement for iron compared to *E. coli* (Figure 4B). The protein components of Bfr complexes in *Synechocystis* have annotated functions linked to iron transport that are absent in *E. coli*. Like Bfr proteins and NQOs mentioned above, conservation analysis of macromolecules allows us to explore the biological processes within cells and how organisms adapt to different environmental demands.

## New roles for proteins related to cell mobility and lipid metabolism

As shown in Figure 3, hypothetical proteins Sll0445, Sll0446, and Sll0447 have putative interactions with pilus assembly proteins and photosystem complexes. Sll0445 contains a Tubulin\_2 domain, and is a member of clan Tubulin (Figure S11A) which serves as cytoskeletal elements vital for cell division and material transport in all eukaryotes [56]. Sll0446 contains a FtsA domain, which is an actin-like ATPase domain, and co-localizes to the septal ring with FtsZ (Figure S11A) [57]. Sll0447 contains a DivIC domain, which is necessary for the formation of both vegetative and sporulation septa (Figure S11A) [58]. To assess these roles, we constructed interruption mutants for each of these three genes, with the insertion of a chloramphenicol-resistance cassette ( $\text{Cm}^R$ ) into their open reading frames (ORFs) (Figure S11B). Then the abilities of phototactic motility were tested and compared across the  $\Delta\text{sll0445}$ ,  $\Delta\text{sll0446}$ ,  $\Delta\text{sll0447}$ , and the wild-type (WT) strain. Under the unidirectional illumination, the WT strain showed obvious movement tendency toward the light, while the  $\Delta\text{sll0445}$ ,  $\Delta\text{sll0446}$ , and  $\Delta\text{sll0447}$  mutants exhibited impaired phototaxis (Figure 5A). Moreover, a previous study showed that the expression level of *sll0447* was decreased in a mutant of *sycr1* [42], a gene involved in phototactic movement [59], indicating that *sll0447* was regulated by *Sycr1* and influenced by cell motility.

The hypothetical proteins Sll0445, Sll0446, and Sll0447 not only formed protein complexes with pilus assembly proteins, but also interacted with photosystem complexes. Targeted removal of these genes from *Synechocystis* genome can affect electron transport of PSII under the optimal condition or low temperature (20 °C) (Figure 5B and C). *Synechocystis* exhibits a typical fluorescence induction polyphasic rise called the OJIP curve, which is similar to previous descriptions in plants, green algae, and cyanobacteria [60]. As shown in Figure 5B and C, the three mutants showed a sharp accumulation of fluorescence at phase J relative to the WT strain, suggesting that the reduction rate of  $\text{Q}_A$  and the oxidation rate of  $\text{Q}_A^-$  were influenced by deletion of *sll0445*, *sll0446*, and *sll0447*.

While these results demonstrate that the proteins encoded by *sll0445*, *sll0446*, and *sll0447* are necessary for the optimal function of photosystem and cell motility, it is still noteworthy that the pilus assembly proteins are distributed on the plasma membrane and the photosynthetic proteins are localized on the thylakoid membrane. Notably, part of the respiratory electron transport chain in *Synechocystis* is located in the thylakoid membrane and partially overlapped with the photosynthetic electron transport chain [49]. In our dataset, the PSI subunits form a complex with NADH dehydrogenase as part of the respiratory chain. The main purpose of *Synechocystis* motility is to obtain plenty of light, which consumes much energy during chemotaxis. Presumably, Sll0445, Sll0446, and Sll0447 link the structure of the thylakoid membrane with the plasma membrane to adjust the capture of light by the photosystem and chemotaxis.

As shown in Figure 3, the histidine kinase Sll1334 interacted with acetyl coenzyme A carboxylase (ACC). Sll1334 contains a GAF domain, which can sense and respond to light (Figure S11A) [61]. We observed that the transcript levels of the ACC subunits were up-regulated in the *sll1334* interruption

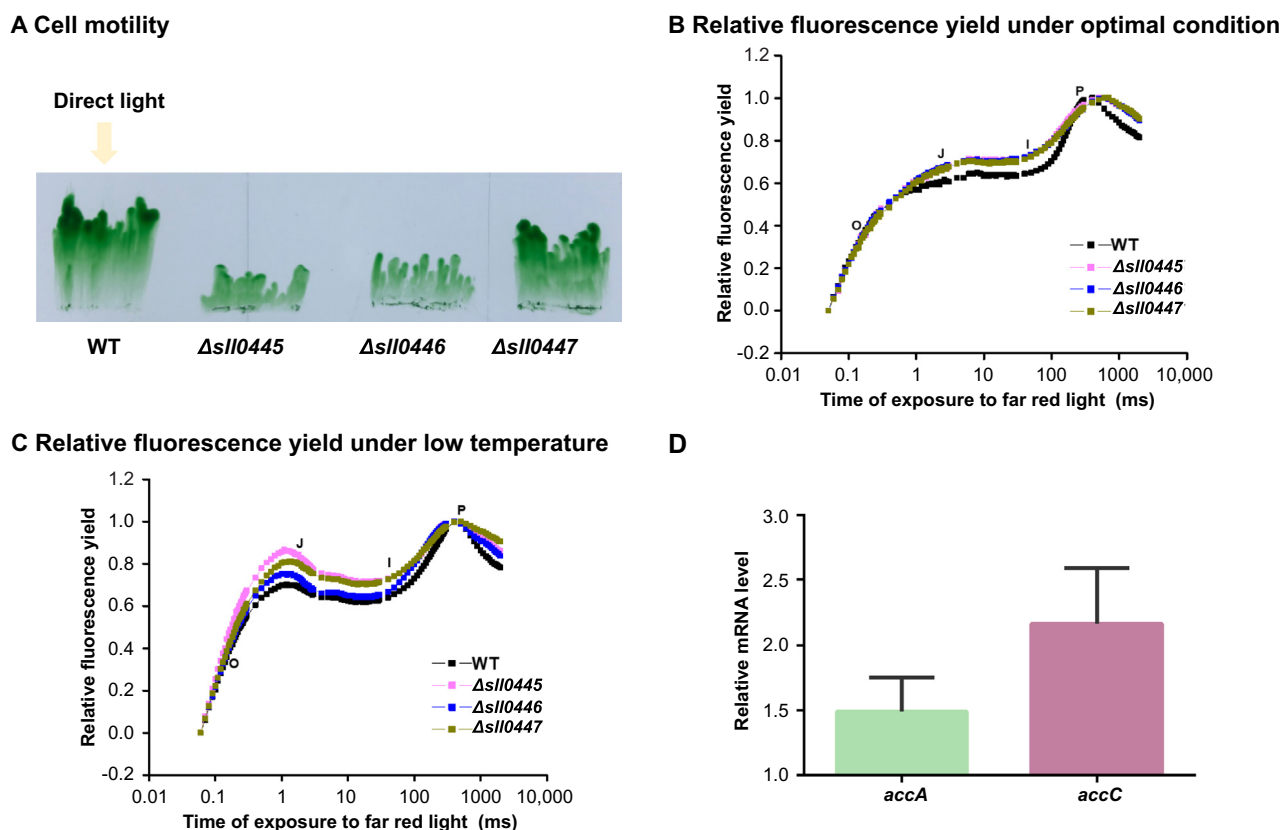


**Figure 5** Validation of protein new functions related to cell motility and lipid metabolism

**A.** The motility states of WT and mutants under unidirectional illumination (white light). The yellow arrow indicates the direction of the light source. **B.** and **C.** OJIP curve under the optimal condition or low temperature (20 °C). The J, I, and P steps occurred at about 2 ms, 30 ms, and 400 ms, respectively. O, origin (minimal fluorescence); P, peak (maximum fluorescence); J and I, inflection points between the O and P levels. **D.** qRT-PCR analysis showing the relative transcript levels of *accA* and *accC* (two genes encoding ACC subunits) in the *Asll1334* mutant compared to those in the WT strain. Ct-values for each gene were normalized to that of *rnpB*. WT, wild-type; ACC, acetyl coenzyme A carboxylase.

mutant (*Asll1334*) as compared with a WT parental strain (Figure 5D). The ACC complex catalyzes acetyl-CoA to form malonyl-CoA, which is part of lipid metabolism conserved across species [62]. Okada et al. have reported that *sll1334* may function as a suppressive regulator in this cascade, influencing cell growth and gene expression involved in glycometabolism under dark conditions [63]. The mechanism is still unclear as to how cyanobacteria adapt to dark conditions and use glucose as the carbon source for growth. However, our results may provide new insight into this process. Carbohydrate and lipid metabolisms drive central metabolism in living cells and have a close relationship with each other to control basic vital activities. Okada et al. found that *sll1330*, which encodes a histidine kinase, is located at the upstream of *sll1334* and influences the expression of *sll1334* [64]. Notably, *Asll1330* and *Asll1334* mutants did not grow well either under light activated heterotrophic or dark heterotrophic conditions as compared to the WT strain. However, they could grow as well as the WT strain under photoautotrophic conditions [63,64]. These results indicate that carbohydrate and lipid metabolisms in *Synechocystis* are regulated by *Sll1330* and *Sll1334*, and that light is an essential factor influencing this process.

Cyanobacteria can produce different bilin-binding photoreceptors when sensing various wavelengths of light, which adjust many essential cellular processes like growth, phototaxis, and photosynthesis to environmental light conditions [61]. The N-terminal region of photoreceptors was found as the photosensory module consisting of a 'knotted' structure including a GAF domain, a PAS domain, and a PHY domain, but not all proteins with a GAF domain are photoreceptors. Thus, further confirmation is needed to determine whether *Sll1334* is a photoreceptor and how it regulates the ACC complex expression by sensing light.

#### Integrative model derived from network systems biology

Through integrating our data with the cyanobacterial metabolism pathway, we depicted a more comprehensive working model of phototaxis regulation, PSII assembly, and physiological metabolism in *Synechocystis* (Figure 6). Light is one of the essential elements to sustain life, especially for cyanobacteria and green plants that fix carbon from the outer environment by photosynthesis. To obtain enough light, cyanobacteria have been evolved with multiple abilities to adapt to light changes. For example, light energy can be harvested by large antenna



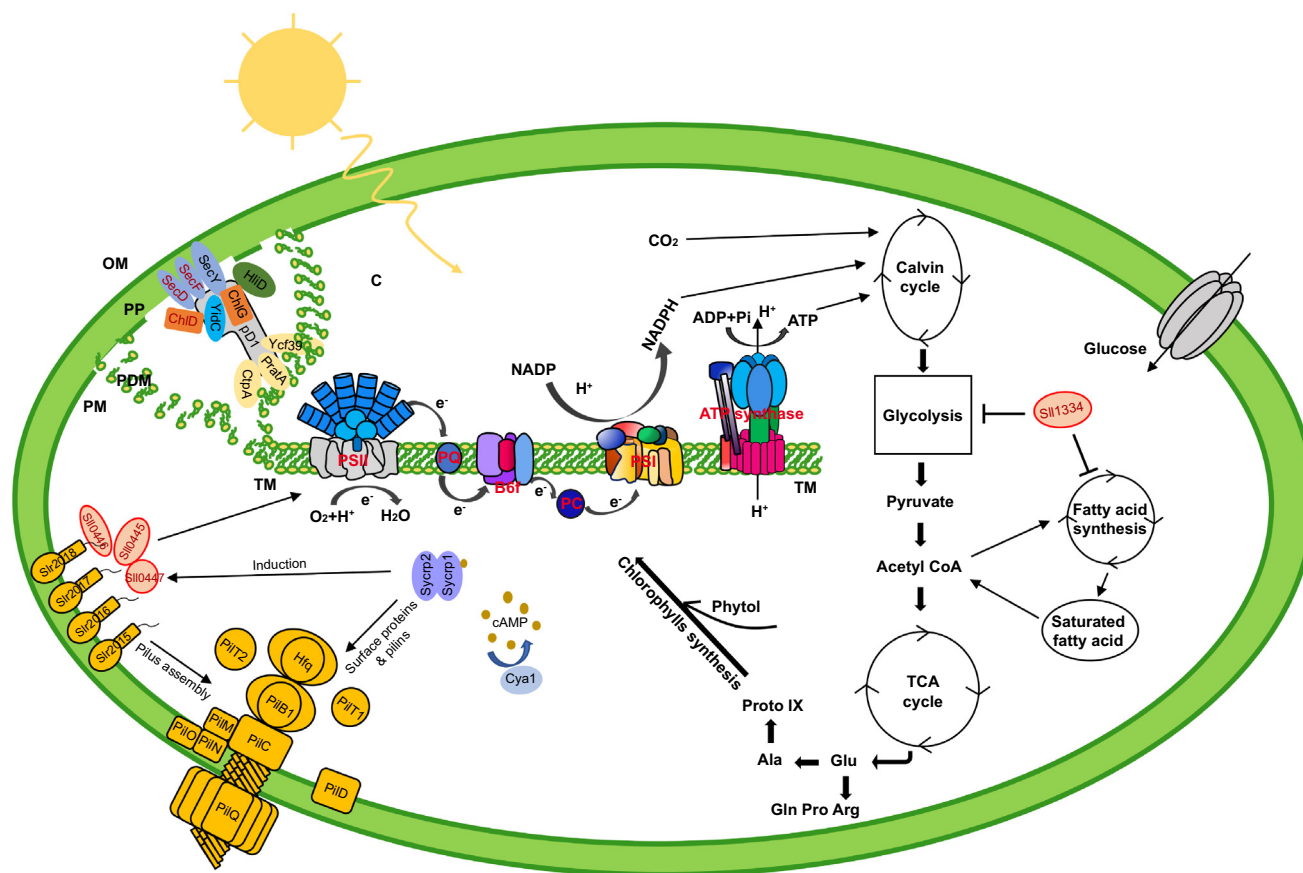


**Figure 6** The model of cyanobacterial phototaxis regulation

The model is based on our data (red color) and public knowledge, showing the phototaxis assembly and how it is influenced by the structure of pilus and carbon metabolism. Proteins SecD, SecF, and ChlD present a good elution profiling with PSII assembly proteins, indicating that Sec complexes and ChlD might play a critical role in the maturation of PSII. The hypothetical proteins SII0445, SII0446, and SII0447 are induced by cAMP receptor protein Sycr1 and interact with pilus assembly proteins to regulate cell motility. These hypothetical proteins can also interact with photosynthetic core proteins, revealing a close relationship between photosynthesis and cell motility in *Synechocystis*. SII1334 can regulate glucolipid metabolism and may have an important role in controlling the utilization of sugars and lipids during heterotrophic growth, thereby affecting photosynthesis. pD1, precursor of D1; C, cytoplasm; L, lumen; OM, outer membrane; PDM, PratA-defined membrane; PM, plasma membrane; PP, periplasm; TM, thylakoid membrane.

complexes — phycobilisomes, while phototaxis allows *Synechocystis* to locate an ideal place to collect light [16,65]. Phototaxis is influenced and regulated by light, the concentration of cAMP, and the structure of pilus in *Synechocystis* [16]. Slr2015–Slr2018 is one class of proteins involved in the process of pilus assembly and can be induced by cAMP receptor protein Sycr1 [42]. The hypothetical proteins SII0445, SII0446, and SII0447 are induced by Sycr1 and interact with pilus assembly proteins, Slr2015, and Slr2018 to regulate cell motilities (Figure S8) [42]. Moreover, SII0445, SII0446, and SII0447 influence photosynthesis through interactions with photosynthetic core proteins, revealing a close relationship between photosynthesis and cell motility in *Synechocystis* (Figure 5B and C).

We also provide more detailed information during the PSII assembly process by combining our predicted PPIs with previously published data (Figure 6). Biogenesis of PSII requires coordinated incorporation of at least 20 polypeptide subunits and a range of organic and inorganic cofactors [14]. Some of these components are well understood during the pratA-dependent PSII assembly process. For example, SecY, YidC,

and CtpA facilitate D1 maturation from pD1; proteins ChlG, HliD, and Ycf39 are involved in the process of delivering the chlorophyll to new D1 or pD1 [34,66,67]. In addition, we observed SecD, SecF, and ChlD co-purifying with these proteins, indicating that Sec complexes and ChlD might play a critical function in the maturation of PSII during the pratA-dependent PSII assembly process (Figure 6).

*Synechocystis* can survive under photoautotrophic or heterotrophic growth conditions. The protein SII1334 can regulate the expression of genes involved glucolipid metabolism. Its GAF domain may have an important role in controlling the utilization of sugars and lipids during heterotrophic growth.

Taken together, these proteins expand our understanding of the regulation of cell motility, PSII assembly, and glucolipid metabolism in *Synechocystis*.

## Conclusion

In this study, by combining CoFrac-MS and quantitative proteomics strategies, we predict 291 protein complexes consisting

of 24,092 highly confident PPIs in *Synechocystis*, which is the largest PPI dataset for this species ever reported. This comprehensive PPI information greatly enhances the basic understanding of the molecular architecture and mechanisms of the photosynthesis machinery as well as other fundamental modules in cyanobacteria.

From the predicted PPIs, most of the proteins tend to have lower degrees involved in metabolic regulation, whereas the proteins with higher degrees are endowed with more basic and conserved functions in *Synechocystis*. By separating photosynthetic protein interaction networks from whole PPIs, we elucidate how photosynthetic proteins connect with other functional units and influence disparate biological processes. By comparing protein complexes in *Synechocystis* with other species, including *A. thaliana*, *E. coli*, *H. sapiens*, and *S. cerevisiae*, we observe macromolecular evolution and functional variations in different species. For example, the change of NQO components in different species may reflect that photosynthetic organisms, like *Synechocystis* and *A. thaliana*, have to undertake the process of photosynthesis and recovery from photosynthetic damage. According to the predicted complexes, the hypothetical proteins SII0445, SII0446, and SII0447 were found to build a functional connection between photosynthesis and cell motility. The photosynthetic apparatus serves as a regulator in the energy metabolic process in living cells. Photosynthesis has a close relationship with chemotaxis, because one of the primary purposes of cell motility is to maximize light exposure so that photosynthesis can tap light energy to fix CO<sub>2</sub> to provide energy for cellular processes. Moreover, expression of the ACC complex was up-regulated when the new component SII1334 was depleted. Cyanobacteria are considered as a promising organism for producing biofuels, but current productivity still needs further improvement. Since SII1334 was found to be a negative regulator of glycolipid metabolism, our work suggests new avenues to improve biofuel productivities by genetic modification.

In summary, the global landscape of native protein complexes in *Synechocystis* provides a valuable resource for researchers to find and determine new and promising macromolecules for further investigations. It also expands our knowledge of the functional interaction network that governs the molecular biology of cyanobacteria.

## Materials and methods

### Growth condition and protein extraction

*Synechocystis* strain was grown in liquid BG11 medium at 30 °C in the light (30 μmol·m<sup>-2</sup>·s<sup>-1</sup>). The cells were collected by centrifugation (6000 g at 4 °C for 5 min) when grew to the exponential phase (OD<sub>730</sub> = 0.8–1). The cells were lysed with lysis buffer containing 20 mM Tris-HCl (pH 7.5), 150 mM NaCl, 1% DDM (Catalog No. D4641, Merck, Darmstadt, Germany), and Complete Protease Inhibitors EDTA-free (Catalog No. 4693124001, Roche, Basel, Switzerland), and then sonicated (5 s on, 10 s off) for about 5 min on ice with an output of 135 W. The cell debris was discarded by centrifugation (12,000 g at 4 °C for 10 min). The protein concentration of each sample was measured using the Bradford assay.

### SEC, IEX, and SDGC

*Synechocystis* cell lysates were fractionated by SEC and IEX on an Ultimate 3000 HPLC system (ThermoFisher Scientific, Bremen, Germany). For SEC, the lysates were injected (350 μl per injection) onto MAbPac SEC-1 (5 μm, 300 mm × 4.0 mm; ThermoFisher Scientific) or Superose 6 10/300GL column (GE Life Sciences). There were 24 fractions collected by using MAbPac SEC-1, with a flow rate of 0.2 ml/min, and 45 fractions collected by using Superose 6 10/300GL column, with a flow rate of 0.3 ml/min. Protein standards (thyroglobulin, BSA, Albumin egg, and myoglobin) were analyzed with the same method to obtain the approximate MW range across fractions. For IEX, the ion-exchange column (12 μm, 200 mm × 4.6 mm, 1500 Å; Columnex, San Diego, CA) was used, and a 110 min salt gradient (0.12–1.2 M NaCl) was used to collect 43 fractions. The elution buffer A containing 10 mM Tris-HCl (pH 7.6), 0.5 mM DTT, and 5% glycerin, while elution buffer B with additional 1.2 M NaCl. For SDGC, lysates were loaded onto a 12 ml 15%–70% (w/v) linear sucrose gradient, which were then centrifuged at 160,000 g at 4 °C for 16 h in a Beckman MLS-50 rotor (Beckman-Coulter, CA), and 24 fractions were collected. In total, 181 fractions were collected.

### APMS

The target protein was combined with a green fluorescent protein (GFP) at its C-terminus. Cell lysate containing the GFP-tagged protein was subjected to affinity purification by using Anti-GFP antibody (Catalog No. ab290, Abcam, Cambridgeshire, UK). The process of antibody purification was carried out using GenScript Protein A MagBeads (Catalog No. L00273, GenScript, Piscataway, NJ) according to the manufacturer's instructions. Then, the sample was detected by MS.

### Trypsin digestion and peptide clean up

Proteins from all HPLC fractions were precipitated with 10% trichloroacetic acid at 4 °C overnight and dissolved in 50 mM ammonium bicarbonate. Trypsin (Catalog No. V5113, Promega, Madison, WI) was added at the ratio of 1:50 and incubated overnight at 37 °C. Each fraction was desalted using ZipTip C18 plates (Catalog No. ZTC18S960, Millipore, Darmstadt, Germany). Peptides were dried using a Labconco evaporator and then resuspended in 0.1% formic acid for further analyses.

### Nano-LC-MS/MS analysis

The peptides were dissolved in 0.1% formic acid, and analyzed using Q-Exactive Plus Orbitrap mass spectrometer (ThermoFisher Scientific). Peptides in 0.1% formic acid were separated on a C18 nano-trap column at a flow rate of 500 nl/min. Peptides were ionized at 2.0 kV. The precursor ions were fragmented by using high energy collision induced dissociation (HCD). The MS/MS spectra of the top 20 most intense signals were acquired by using a data-dependent method. The dynamic exclusion duration was set as 40 s and 5 × 10<sup>4</sup> ions

were set to generate MS/MS spectra in the automatic gain control (AGC). The Proteome Discoverer version 2.1 was used to retrieve the RAW data using a target-decoy based strategy, supplied with the *Synechocystis* 3508 reference protein (UP000001425) from the UniProt database. Up to 2 missed cleavages were allowed.

### Data analysis

R Language and Python scripts were applied to data analysis. The elution profiles for individual proteins were normalized and smoothed by using scale command in R Language. The Mapp of all proteins identified in our dataset was calculated similarly as previously described [26]. After that, the ratio of Mapp to Mmono was calculated, and the value of Rapp (Mapp/Mmono) can effectively reflect the oligomerization state of proteins during the protein separation process. The protein with a value of  $Rapp \geq 2$  implies an oligomerization state, while  $Rapp \leq 0.5$  means that it may be degraded during the protein extraction process and would be discarded in subsequent analysis. The protein with a value of  $0.5 < Rapp < 2$  exists as a monomeric state.

### Machine learning

We used EPIC software for automated scoring of our data for the large-scale determination of high-confidence physical interaction networks and macromolecular assemblies from diverse biological specimens. This software package can be obtained from <https://github.com/BaderLab/EPIC>. Protein pairs were scored based on five features: MI, Bayes Correlation, Jaccard, Pearson Correlation Coefficient, and Apex Score. We manually collected a data set of “gold standard” protein complexes by the reference database (UniProt) for machine learning analysis, which contains 48 conserved true positive protein complexes. Positive PPIs are defined if they appear in the same protein complex, while the components of negative PPIs are from proteins existing in the different protein complexes. Then the positive and negative PPIs were used to train the machine learning classifier. The protein pairs with elution profile similarity scores more than 0.5 were required, and the proteins that used for machine learning were detected with not less than 2 peptide spectrum matches in at least one of the experiments.

### Construction of plasmids

Single mutants of the *sll0445–sll0447* gene cluster and *sll1334* were generated by inserting a  $Cm^R$  into their ORFs. For APMS, GFP-tag was added to the C-termini of *sll0445* and *sll0149* in the genome. The targeted gene and its flanking sequences were amplified by PCR with *Synechocystis* chromosome DNA as the template and cloned into the pMD18-T vector (Catalog No. D101A, Takara, Japan). The insertion mutants were verified by PCR (Figure S11B). Primers used for mutant construction are as follows: M\_ *sll0445*up, 5'-GTT CAGCGGTGATGAGTVG-3'; M\_ *sll0445*down, 5'-GTAAAT CAAACAGGGCATG-3'; M\_ *sll0446*up, 5'-TGTGGCCTA TACAATGTCCCAG-3'; M\_ *sll0446*down, 5'-AAGATATT TCTTCCAGCAAATGG-3'; M\_ *sll0447*up, 5'-ATCTCGTAT TAAGAAAGCTTG-3'; M\_ *sll0447*down, 5'-TGAGCATAA ACTGGACTAATG-3'; M\_ *sll1334*up, 5'-AGACGGTTA

GAACCAACAGTCACTG-3'; M\_ *sll1334*down, 5'-ACAATT TGTAAGCCCTGGCGAACG-3'.

### Cell motility assay and measurement of photosynthetic activity

Phototactic movement was tested according to Wilde and colleagues [68]. The strains were grown on solid BG11 medium containing 0.3% sodium thiosulfate, 8 mM TES (pH 8.0), 0.8% agar, and 5 mM glucose, under unidirectional illumination with light intensity at  $1\text{--}5 \mu\text{mol photons m}^{-2}\cdot\text{s}^{-1}$  and the movements were recorded at day 6. The modification of PSII photochemistry in *Synechocystis* was evaluated by OJIP curve, measured by Plant Efficiency Analyzer (Hansatech, Germany).

### RNA isolation and qRT-PCR analysis

About 50 ml of *Synechocystis* grown in BG11 was collected by centrifugation at 4 °C and the total RNA was extracted using the TRIzol Reagent (Catalog No. 15596-026, Invitrogen, Waltham, MA). The cDNA was synthesized with the Perfect Real Time Kit (Catalog No. RR047A, Takara, Japan), and used as a template for qRT-PCR analysis. RNase P subunit B (*rnpB*) was used as an internal control. Primers used for qRT-PCR are as follows: *accA*up, 5'-AAATGTTTCGGTTAGATGT CC-3'; *accA*down, 5'-CCAAAGAATAGCCGCACA-3'; *accC*up, 5'-TTTGGTGGATGGTAACGG-3'; *accC*down, 5'-TGGCGGAAGCGGAGTTTT-3'; *rnpB*up, 5'-ACCGCTTG AGGAATTTGGTA-3'; *rnpB*down, 5'-TTAGTCGTAAGCC GGGTTCT-3'.

### Data availability

All LC-MS/MS raw data related to this work have been deposited to the ProteomeXchange Consortium via the iProX partner repository (ProteomeXchange: PXD015948; iProX: IPX0001620001), which are publicly accessible at <http://proteomecentral.proteomexchange.org> and <https://www.iprox.org>, respectively.

### CRedit author statement

**Chen Xu:** Investigation, Visualization, Writing - original draft. **Bing Wang:** Resources. **Lin Yang:** Visualization. **Lucas Zhongming Hu:** Software. **Lanxing Yi:** Investigation. **Yaxuan Wang:** Investigation. **Shenglan Chen:** Investigation. **Andrew Emili:** Writing - review & editing. **Cuihong Wan:** Conceptualization, Supervision, Writing - review & editing. All authors have read and approved the final manuscript.

### Competing interests

The authors declare no competing interests to this work. We declare that we do not have any commercial or associative interest that represents a conflict of interest in connection with the work submitted.

### Acknowledgments

This work was funded by the Young Thousand Talents Program. We thank Prof. Baosheng Qiu, Prof. Haibo Jiang, and

Dr. Guozheng Dai (Central China Normal University) for providing algal, cloning vectors, and technical guidance. We would like to particularly thank Prof. Feng Ge (Institute of Hydrobiology, Chinese Academy of Sciences) for the valuable discussion. We also thank other members of the Wan lab for all their support to this project.

## Supplementary material

Supplementary data to this article can be found online at <https://doi.org/10.1016/j.gpb.2020.06.020>.

## ORCID

ORCID 0000-0002-5075-7154 (Chen Xu)  
 ORCID 0000-0003-3050-4712 (Bing Wang)  
 ORCID 0000-0003-2277-5440 (Lin Yang)  
 ORCID 0000-0002-1781-9341 (Lucas Zhongming Hu)  
 ORCID 0000-0003-2974-1745 (Lanxing Yi)  
 ORCID 0000-0002-4709-8637 (Yaxuan Wang)  
 ORCID 0000-0001-6566-0243 (Shenglan Chen)  
 ORCID 0000-0001-8995-246X (Andrew Emili)  
 ORCID 0000-0002-6028-3239 (Cuihong Wan)

## References

- [1] Falcon LI, Magallon S, Castillo A. Dating the cyanobacterial ancestor of the chloroplast. *ISME J* 2010;4:777–83.
- [2] Martin W, Rujan T, Richly E, Hansen A, Cornelsen S, Lins T, et al. Evolutionary analysis of, cyanobacterial, and chloroplast genomes reveals plastid phylogeny and thousands of cyanobacterial genes in the nucleus. *Proc Natl Acad Sci U S A* 2002;99:12246–51.
- [3] Schirmer BE, de Vos JM, Antonelli A, Bagheri HC. Evolution of multicellularity coincided with increased diversification of cyanobacteria and the Great Oxidation Event. *Proc Natl Acad Sci U S A* 2013;110:1791–6.
- [4] Xiong Q, Chen Z, Ge F. Proteomic analysis of post translational modifications in cyanobacteria. *J Proteomics* 2016;134:57–64.
- [5] Hohmann-Marriott MF, Blankenship RE. Evolution of photosynthesis. *Annu Rev Plant Biol* 2011;62:515–48.
- [6] Kaneko T, Stato S, Kotani H, Kaneko A, Asamizu E, Nakamura Y, et al. Sequence analysis of the genome of the unicellular cyanobacterium *Synechocystis* sp. strain PCC 6803. II. Sequence determination of the entire genome and assignment of potential protein-coding regions. *DNA Res* 1996;3:109–36.
- [7] Gao L, Wang JL, Ge HT, Fang LF, Zhang YY, Huang XH, et al. Toward the complete proteome of *Synechocystis* sp. PCC 6803. *Photosynth Res* 2015;126:203–19.
- [8] Castielli O, De la Cerda B, Navarro JA, Hervas M, De la Rosa MA. Proteomic analyses of the response of cyanobacteria to different stress conditions. *FEBS Lett* 2009;583:1753–8.
- [9] Typas A, Sourjik V. Bacterial protein networks: properties and functions. *Nat Rev Microbiol* 2015;13:559–72.
- [10] Lv Q, Ma WM, Liu H, Li J, Wang H, Wang H, et al. Genome-wide protein-protein interactions and protein function exploration in cyanobacteria. *Sci Rep* 2015;5:1–12.
- [11] Kim WY, Kang S, Kim BC, Oh J, Cho S, Bhak J, et al. SynchoNET: integrated protein-protein interaction database of a model cyanobacterium *Synechocystis* sp. PCC 6803. *BMC Bioinformatics* 2008;9:S20.
- [12] Michaut M, Kerrien S, Montecchi-Palazzi L, Chauvat F, Cassier-Chauvat C, Aude JC, et al. InteroPORC: automated inference of highly conserved protein interaction networks. *Bioinformatics* 2008;24:1625–31.
- [13] Sato S, Shimoda Y, Muraki A, Kohara M, Nakamura Y, Tabata S. A large-scale protein-protein interaction analysis in *Synechocystis* sp. PCC 6803. *DNA Res* 2007;14:207–16.
- [14] Heinz S, Liauw P, Nickelsen J, Nowaczyk M. Analysis of photosystem II biogenesis in cyanobacteria. *Biochim Biophys Acta* 2016;1857:274–87.
- [15] Nickelsen J, Rengstl B. Photosystem II assembly: from cyanobacteria to plants. *Annu Rev Plant Biol* 2013;64:609–35.
- [16] Schuergers N, Mullineaux CW, Wilde A. Cyanobacteria in motion. *Curr Opin Plant Biol* 2017;37:109–15.
- [17] Maier B, Wong GCL. How bacteria use type IV pili machinery on surfaces. *Trends Microbiol* 2015;23:775–88.
- [18] Babu M, Bundalovic-Torma C, Calmettes C, Phanse S, Zhang Q, Jiang Y, et al. Global landscape of cell envelope protein complexes in *Escherichia coli*. *Nat Biotechnol* 2017;36:103–12.
- [19] Hein MY, Hubner NC, Poser I, Cox J, Nagaraj N, Toyoda Y, et al. A human interactome in three quantitative dimensions organized by stoichiometries and abundances. *Cell* 2015;163:712–23.
- [20] Wan C, Borgeson B, Phanse S, Tu F, Drew K, Clark G, et al. Panorama of ancient metazoan macromolecular complexes. *Nature* 2015;525:339–44.
- [21] Rolland T, Tasan M, Charlotiaux B, Pevzner SJ, Zhong Q, Sahni N, et al. A proteome-scale map of the human interactome network. *Cell* 2014;159:1212–26.
- [22] Larance M, Lamond AI. Multidimensional proteomics for cell biology. *Nat Rev Mol Cell Biol* 2015;16:269–80.
- [23] Crozier TWM, Tinti M, Larance M, Lamond AI, Ferguson MAJ. Prediction of protein complexes in *Trypanosoma brucei* by protein correlation profiling mass spectrometry and machine learning. *Mol Cell Proteomics* 2017;16:2254–67.
- [24] Kirkwood KJ, Ahmad Y, Larance M, Lamond AI. Characterization of native protein complexes and protein isoform variation using size-fractionation-based quantitative proteomics. *Mol Cell Proteomics* 2013;12:3851–73.
- [25] Havugimana PC, Hart GT, Nepusz T, Yang H, Turinsky AL, Li Z, et al. A census of human soluble protein complexes. *Cell* 2012;150:1068–81.
- [26] Aryal UK, McBride Z, Chen D, Xie J, Szymanski DB. Analysis of protein complexes in *Arabidopsis* leaves using size exclusion chromatography and label-free protein correlation profiling. *J Proteomics* 2017;166:8–18.
- [27] Aryal UK, Xiong Y, McBride Z, Kihara D, Xie J, Hall MC, et al. A proteomic strategy for global analysis of plant protein complexes. *Plant Cell* 2014;26:3867–82.
- [28] Hu LZ, Goebels F, Tan JH, Wolf E, Kuzmanov U, Wan C, et al. EPIC: software toolkit for elution profile-based inference of protein complexes. *Nat Methods* 2019;16:737–42.
- [29] Ouma WZ, Pogacar K, Grotewold E. Topological and statistical analyses of gene regulatory networks reveal unifying yet quantitatively different emergent properties. *PLoS Comput Biol* 2018;14:1–17.
- [30] Calderone A, Castagnoli L, Cesareni G. mentha: a resource for browsing integrated protein-interaction networks. *Nat Methods* 2013;10:690–1.
- [31] Feder ME, Hofmann GE. Heat-shock proteins, molecular chaperones, and the stress, and the stress response: evolutionary and ecological physiology. *Ann Rev Physiol* 1999;61:243–82.
- [32] Barabasi AL, Oltvai ZN. Network biology: understanding the cell's functional organization. *Nat Rev Genet* 2004;5:101–13.
- [33] Linhartova M, Bucinska L, Halada P, Jecmen T, Setlik J, Komenda J, et al. Accumulation of the type IV prepilin triggers degradation of SecY and YidC and inhibits synthesis of Photosystem II proteins in the cyanobacterium *Synechocystis* PCC 6803. *Mol Microbiol* 2014;93:1207–23.



- [34] Chidgey JW, Linhartova M, Komenda J, Jackson PJ, Dickman MJ, Canniffe DP, et al. A cyanobacterial chlorophyll synthase-HliD complex associates with the Ycf39 protein and the YidC/Alb3 insertase. *Plant Cell* 2014;26:1267–79.
- [35] Gao LY, Ge HT, Huang XH, Liu KH, Zhang YY, Xu W, et al. Systematically ranking the tightness of membrane association for peripheral membrane proteins (PMPs). *Mol Cell Proteomics* 2015;14:340–53.
- [36] Nepusz T, Yu H, Paccanaro A. Detecting overlapping protein complexes in protein-protein interaction networks. *Nat Methods* 2012;9:471–2.
- [37] Behler J, Sharma K, Reimann V, Wilde A, Urlaub H, Hess WR. The host-encoded RNase E endonuclease as the crRNA maturation enzyme in a CRISPR–Cas subtype III-Bv system. *Nat Microbiol* 2018;3:367–77.
- [38] Scholz I, Lange SJ, Hein S, Hess WR, Backofen R. CRISPR-Cas systems in the cyanobacterium *Synechocystis* sp. PCC 6803 exhibit distinct processing pathways involving at least two Cas6 and a Cmr2 protein. *PLoS One* 2013;8:e56470.
- [39] Hale CR, Zhao P, Olson S, Duff MO, Graveley BR, Wells L, et al. RNA-guided RNA cleavage by a CRISPR RNA-Cas protein complex. *Cell* 2009;139:945–56.
- [40] Wegener KM, Welsh EA, Thornton LE, Keren N, Jacobs JM, Hixson KK, et al. High sensitivity proteomics assisted discovery of a novel operon involved in the assembly of photosystem II, a membrane protein complex. *J Biol Chem* 2008;283:27829–37.
- [41] Luck K, Sheynkman GM, Zhang I, Vidal M. Proteome-scale human interactomics. *Trends Biochem Sci* 2017;42:342–54.
- [42] Yoshimura H, Yanagisawa S, Kanehisa M, Ohmori M. Screening for the target gene of cyanobacterial cAMP receptor protein SYCRP1. *Mol Microbiol* 2002;43:843–53.
- [43] Bhaya D, Takahashi A, Shahi P, Grossman AR. Novel motility mutants of *Synechocystis* strain PCC 6803 generated by *in vitro* transposon mutagenesis. *J Bacteriol* 2001;183:6140–3.
- [44] Olsen GJ, Woese CR, Overbeek R. The winds of (evolutionary) change: breathing new life into microbiology. *J Bacteriol* 1994;176:1–6.
- [45] Woese C. Bacterial evolution. *Microbiol Rev* 1987;51:221–71.
- [46] Gao F, Zhao J, Wang X, Qin S, Wei L, Ma W. NdhV is a subunit of NADPH dehydrogenase essential for cyclic electron transport in *Synechocystis* sp. strain PCC 6803. *Plant Physiol* 2016;170:752–60.
- [47] Gao F, Zhao J, Chen L, Battchikova N, Ran Z, Aro EM, et al. The NDH-1L-PSI supercomplex is important for efficient cyclic electron transport in cyanobacteria. *Plant Physiol* 2016;172:1451–64.
- [48] Matsushita K, Ohnishi T, Kaback H. NADH-ubiquinone oxidoreductases of the *Escherichia coli* aerobic respiratory chain. *Biochemistry* 1987;26:7732–7.
- [49] Peschek GA, Obinger C, Paumann M. The respiratory chain of blue-green algae (cyanobacteria). *Physiol Plant* 2004;120:358–69.
- [50] Ingledew W, Poole R. The respiratory chains of *Escherichia coli*. *Microbiol Rev* 1984;48:222–71.
- [51] Melo AM, Bandejas TM, Teixeira M. New insights into type II NAD(P)H:quinone oxidoreductases. *Microbiol Mol Biol Rev* 2004;68:603–16.
- [52] Apel K, Hirt H. Reactive oxygen species: metabolism, oxidative stress, and signal transduction. *Annu Rev Plant Biol* 2004;55:373–99.
- [53] Mittler R. Oxidative stress, antioxidants and stress tolerance. *Trends Plant Sci* 2002;7:405–10.
- [54] Shcolnick S, Keren N. Metal homeostasis in cyanobacteria and chloroplasts. Balancing benefits and risks to the photosynthetic apparatus. *Plant Physiol* 2006;141:805–10.
- [55] Morel FMM, Price NM. The biogeochemical cycles of trace metals in the oceans. *Science* 2003;300:944–7.
- [56] Nogales E, Wolf SG, Downing KH. Structure of the  $\alpha\beta$  tubulin dimer by electron crystallography. *Nature* 1998;391:199–203.
- [57] Ent FVD, Löwe J. Crystal structure of the cell division protein FtsA from *Thermotoga maritima*. *EMBO J* 2000;19:5300–7.
- [58] Noirclerc-Savoie M, Le Gouellec A, Morlot C, Dideberg O, Vernet T, Zapun A. *In vitro* reconstitution of a trimeric complex of DivIB, DivIC and FtsL, and their transient co-localization at the division site in *Streptococcus pneumoniae*. *Mol Microbiol* 2005;55:413–24.
- [59] Yoshihara S, Ikeuchi M. Phototactic motility in the unicellular cyanobacterium *Synechocystis* sp. PCC 6803. *Photoch Photobio Sci* 2004;3:512–8.
- [60] Qiu B, Zhang A, Zhou W, Wei J, Dong H, Liu Z. Effects of potassium on the photosynthetic recovery of the terrestrial cyanobacterium, *Nostoc Flagelliforme* (Cyanophyceae) during rehydration. *J Phycol* 2004;40:323–32.
- [61] Wiltbank LB, Kehoe DM. Diverse light responses of cyanobacteria mediated by phytochrome superfamily photoreceptors. *Nat Rev Microbiol* 2019;17:37–50.
- [62] Huerlimann R, Heimann K. Comprehensive guide to acetyl-carboxylases in algae. *Crit Rev Biotechnol* 2013;33:49–65.
- [63] Okada K, Horii E, Nagashima Y, Mitsui M, Matsuura H, Fujiwara S, et al. Genes for a series of proteins that are involved in glucose catabolism are upregulated by the Hik8-cascade in *Synechocystis* sp. PCC 6803. *Planta* 2015;241:1453–62.
- [64] Tabei Y, Okada K, Makita N, Tsuzuki M. Light-induced gene expression of fructose 1,6-bisphosphate aldolase during heterotrophic growth in a cyanobacterium, *Synechocystis* sp. PCC 6803. *FEBS J* 2009;276:187–98.
- [65] Tang K, Ding WL, Höppner A, Zhao C, Zhang L, Hontani Y, et al. The terminal phycobilisome emitter, L<sub>CM</sub>: a light-harvesting pigment with a phytochrome chromophore. *Proc Natl Acad Sci U S A* 2015;112:15880–5.
- [66] Sachelaru I, Petriman NA, Kudva R, Kuhn P, Welte T, Knapp B, et al. YidC occupies the lateral gate of the SecYEG translocon and is sequentially displaced by a nascent membrane protein. *J Biol Chem* 2013;288:16295–307.
- [67] Anbudurai P, Mor T, Ohad I, Shestakov S, Pakrasi H. The *ctpA* gene encodes the C-terminal processing protease for the D1 protein of the photosystem II reaction center complex. *Proc Natl Acad Sci U S A* 1994;91:8082–6.
- [68] Wilde A, Fiedler B, Börner T. The cyanobacterial phytochrome Cph2 inhibits phototaxis towards blue light. *Mol Microbiol* 2002;44:981–8.